

# Optimization of state parameters in displacement assisted photon subtracted measurement-device-independent quantum key distribution

Chandan Kumar,<sup>1,\*</sup> Sarbani Chatterjee,<sup>1,†</sup> and Arvind<sup>1,‡</sup>

<sup>1</sup>*Department of Physical Sciences, Indian Institute of Science Education and Research Mohali, Sector 81 SAS Nagar, Punjab 140306 India.*

Non-Gaussian operations, in particular, photon subtraction (PS), have been shown to enhance the performance of various quantum information processing tasks including continuous variable measurement device independent quantum key distribution (CV-MDI-QKD). This work investigates the role of non-Gaussian resource states, namely, the photon subtracted two-mode squeezed coherent (PSTMSC) (which include photon subtracted two-mode squeezed vacuum (PSTMSV) as a special case) states in CV-MDI-QKD. To this end, we derive the Wigner characteristic function for the resource states, from which the covariance matrix and, finally, the secret key rate expressions are extracted. The optimization of the state parameters is undertaken to find the most suitable resource states in this family of states. There have been previous studies on the PSTMSV and PSTMSC states in CV-MDI-QKD that make use of PS operation. We evaluate such proposals and find to our surprise that both PSTMSC and PSTMSV resource states underperform as compared to the TMSV state rendering PS operation and displacement undesirable.

## I. INTRODUCTION

Quantum key distribution (QKD) [1–3] is one of the most developed applications of quantum information science, where two distant parties, Alice and Bob, desire to establish a shared secret key. The field of QKD can be broadly divided into two major categories, discrete variable (DV) QKD [4–7] and continuous variable (CV) QKD [8–13]. CV-QKD offers a higher secret key rate (SKR) than DV-QKD and has gained preference over DV-QKD due to ease in implementation and the possibility of carrying out homodyne and heterodyne measurements with high efficiency. Security aspects of some of these protocols have been analyzed in detail in Refs. [14–18]. Unconditional security of QKD protocols typically requires perfect devices and noiseless channels. In the practical situations where noise is always present and devices are not perfect, security loopholes develop and constructing a fully secure protocol becomes a challenge.

The DV measurement device independent (MDI) QKD protocol, which is based on the concept of entanglement swapping, was proposed to remove all security loopholes arising from the detectors [19, 20]. Soon after, the idea of MDI was extended to CV systems [21–23]. In CV-MDI-QKD protocols, an untrusted third party employs a CV Bell measurement and publicly communicates the results, which leads to sharing of the secret key between the legitimate parties. The SKR obtained in CV-QKD is higher; however, the maximum transmission distance is substantially lower as compared to DV-MDI-QKD.

Typically multimode Gaussian states of the radiation field are used as resource states for general quantum information processing (QIP) tasks and in particular

for CV-MDI-QKD [3, 13]. In order to increase non-classicality and entanglement, non-Gaussian states have been engineered by implementing non-Gaussian operations such as photon subtraction, addition, and catalysis on Gaussian states [24–29]. Such non-Gaussian states have been employed to improve the performances of various QIP protocols such as quantum teleportation [30–37], quantum key distribution [38–43] and quantum metrology [44–53]. These non-Gaussian operations, in particular, the photon subtraction (PS) on two-mode squeezed vacuum (TMSV) and two-mode squeezed coherent (TMSC) states, have been shown to enhance the performance of CV-MDI-QKD protocols [39, 40].

In this work, we undertake to explore the full parameter space of PSTMSC states for their performance of the CV-MDI-QKD protocol. The photon subtracted TMSC (PSTMSC) is a family of states determined by three parameters, namely, variance (squeezing), displacement, and transmissivity of the beam splitter involved in the implementation of the PS operation. We first keep the variance fixed and optimize the SKR with respect to the remaining two state parameters. At fixed high variances, we obtain an improvement in the maximum transmission distance and a significant improvement in the SKR as compared to the results reported earlier [40]. Further, we observe that the PSTMSV states do not provide any advantage either in SKR or maximum transmission distance over the TMSV state, unlike the conclusion drawn in an earlier work [39]. At fixed low variance, the results show that photon subtraction operation does not provide any benefit in terms of higher SKR or transmission distance. Finally, we perform the optimization of SKR with respect to all the three state parameters. In contradiction to several recent papers claiming that photon subtraction and displacement on Alice’s side of the CV-MDI-QKD protocol is advantageous, we conclude that there is no advantage in using photon subtraction and displacement in CV-MDI-QKD protocols.

Our study directly impacts the utility of photon sub-

\* chandan.quantum@gmail.com

† mp18015@iisermohali.ac.in

‡ arvind@iisermohali.ac.in

traction in CV-MDI-QKD protocols [54–56]. Other CV-QKD protocols such as entanglement-based CV-QKD protocol [57], entanglement in the middle CV-QKD protocol [58], virtual post selection based CV-QKD protocol [59] also needs to be optimized with respect to state parameters to assess their utility of photon subtraction.

Exploiting the fact that the introduction of displacement also helps maintain the maximum transmission distance for multi-photon subtracted TMSC states, we propose a new variant of the QKD protocol that simultaneously uses 1-PSTMSC, 2-PSTMSC, 3-PSTMSC and 4-PSTMSC states ( $k$ -PSTMSC state represents  $k$  photon subtracted TMSC state). This enables us to maximize the utilization of resources per trial and consequently leads to a significant enhancement in the key rate. We note that this protocol is efficient at high variance. Our analysis at variance  $V = 15$  shows that using 1-PSTMSC state alone provides a resource utilization of approximately 36%, while using all four PSTMSC states enhances it to approximately 78%.

Other important aspect of the current work is the derivation of the Wigner characteristic function of the PSTMSC states. The elements of the covariance matrix, which are second-order moments of the quadrature operators symmetrized as per the Weyl correspondence rule, can be evaluated by differentiation of the Wigner characteristic function. The Wigner characteristic function, as well as the different moments of the covariance matrix, are provided in a compact form, which will render its applications in other QKD protocols to be convenient.

The article is structured as follows. Section II A contains the derivation of the Wigner characteristic function and the different moments of the covariance matrix of the PSTMSC states. In Sec. II B, we briefly describe the PSTMSC states based CV-MDI-QKD protocol and in Sec. II C, we set up the notations required to evaluate the secret key. In Sec. III, we optimize the SKR with respect to the state parameters. Finally, in Sec. IV, we conclude the main results of the current work and discuss future prospects. In Appendix A, we review the formalism of CV systems and its phase space description.

## II. REVIEW OF CV-MDI-QKD PROTOCOL

In this section, we evaluate the covariance matrix required for the calculation of secret key rate. Further, it provides a brief overview of the entanglement-based CV-MDI-QKD protocol for the PSTMSC state [40] and details its security analysis.

### A. Wigner characteristic function of the PSTMSC state

The schematic for the generation of the PSTMSC state is shown in Fig. 1. The two modes of the TMSC state are labeled as  $A_1$  and  $A_2$  and represented by the quadrature

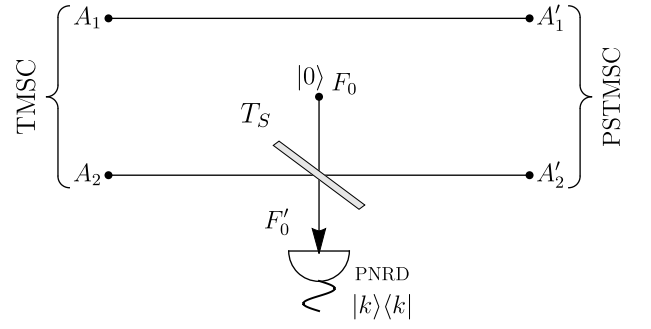


FIG. 1. Schematic for preparation of the PSTMSC state generation from the TMSC state. The mode  $A_2$  of the TMSC state is interfered with the ancillary mode  $F_0$  using a beam splitter. The detection of  $k$  photons at the PNRD represents a successful preparation of a  $k$ -PSTMSC state.

operators  $\hat{q}_1, \hat{p}_1$  and  $\hat{q}_2, \hat{p}_2$ . To generate TMSC state, one begins with two uncorrelated modes, each in a coherent state, represented by the following displacement vector and covariance matrix (in shot noise units):

$$\bar{\xi} = (d, 0, d, 0)^T, \quad \Sigma = \mathbb{1}_4, \quad (1)$$

where  $\mathbb{1}_4$  is the  $4 \times 4$  identity matrix. These modes are sent through a two-mode nonlinear optical down converter to obtain a TMSC state. The displacement vector and covariance matrix transform according to Eq. (A16) given in Appendix A 1 as

$$\bar{\xi} \rightarrow S_{A_1 A_2}(r) \bar{\xi}, \quad \Sigma \rightarrow S_{A_1 A_2}(r) \Sigma S_{A_1 A_2}(r)^T, \quad (2)$$

where  $S_{A_1 A_2}(r)$  is the two mode squeezing operator defined in Eq. (A8). We use the Wigner characteristic function formalism, which turns out to be a convenient and effective approach in calculating the covariance matrix, whose elements are second order moments symmetrized as per the Weyl correspondence rule. The Wigner characteristic function (A14) of the TMSC state evaluates to

$$\begin{aligned} \chi_{A_1 A_2}(\Lambda_1, \Lambda_2) = \exp \left[ -\frac{1}{2} \cosh(2r) (\sigma_1^2 + \sigma_2^2 + \tau_1^2 + \tau_2^2) \right. \\ \left. + \sinh(2r) (\tau_1 \tau_2 - \sigma_1 \sigma_2) + i d e^{-r} (\sigma_1 + \sigma_2) \right]. \end{aligned} \quad (3)$$

We now consider an ancilla mode  $F_0$  represented by the quadrature operators  $(\hat{q}_3, \hat{p}_3)^T$  initialized to the vacuum state. Fred interferes the ancilla mode  $F_0$  with the mode  $A_2$  of the TMSC state received from Alice, with the help of a beam splitter of transmissivity  $T_S$ . The Wigner characteristic function prior to the interference is given by

$$\chi_{A_1 A_2 F_0}(\Lambda) = \chi_{A_1 A_2}(\Lambda_1, \Lambda_2) \chi_{|0\rangle}(\Lambda_3). \quad (4)$$

The action of the beam splitter entangles the input modes and the transformed Wigner characteristic function post the beam splitter interference is given by

$$\chi_{A_1' A_2' F_0'}(\Lambda) = \chi_{A_1 A_2 F_0}([\mathbb{1} \oplus B_{A_2 F_0}(T_S)]^{-1} \Lambda). \quad (5)$$

Now the transformed mode  $F'_0$  is measured using a PNRD, which is described by the POVM  $\{\Pi_k = |k\rangle\langle k|, \mathbb{1} - \Pi_k\}$ . A click of the POVM element  $\Pi_k$  represents a successful  $k$  photon subtraction. The unnormalized Wigner characteristic function of the  $k$ -PSTMSC state is given by

$$\begin{aligned} \tilde{\chi}_{A_1 A'_2}^{(k)}(\Lambda_1, \Lambda_2) &= \frac{1}{\pi} \int d^2 \Lambda_3 \underbrace{\chi_{A'_1 A'_2 F'_0}(\Lambda)}_{\text{Three mode entangled state}} \\ &\times \underbrace{\chi_{|k\rangle}(-\Lambda_3)}_{\text{Projection on } |k\rangle\langle k|}. \end{aligned} \quad (6)$$

To integrate the above equation, we write the Laguerre polynomial occurring in the Wigner characteristic function of the Fock state  $|k\rangle$  as

$$L_k(\tau_3^2 + \sigma_3^2) = \frac{1}{k!} \frac{\partial^k}{\partial u^k} \frac{\partial^k}{\partial v^k} e^{uv+u(\tau_3+i\sigma_3)-v(\tau_3-i\sigma_3)} \Big|_{u=v=0}. \quad (7)$$

Substituting the above in Eq. (6) leads to a Gaussian integral, which evaluates to

$$\begin{aligned} \tilde{\chi}_{A_1 A'_2}^{(k)}(\Lambda_1, \Lambda_2) &= 2z_1 z_2^k \exp[x_1(\sigma_1^2 + \tau_1^2 + \sigma_2^2 + \tau_2^2)] \\ &\times \exp[x_2(\sigma_1\sigma_2 - \tau_1\tau_2) + x_3\sigma_1 + x_4\sigma_2 + x_5] \\ &\times L_k[y_1(\sigma_1^2 + \tau_1^2) + y_2(\sigma_2^2 + \tau_2^2) \\ &+ y_3(\sigma_1\sigma_2 - \tau_1\tau_2) + y_4\sigma_1 + y_5\sigma_2 + y_6], \end{aligned} \quad (8)$$

where the coefficients  $x_i$ ,  $y_i$  and  $z_i$  are given as

$$\begin{aligned} x_1 &= -z_1(\alpha^2 T_S + \beta^2), & y_1 &= 2z_1 T_S \alpha^2, \\ x_2 &= -4z_1 \sqrt{T_S} \alpha \beta, & y_2 &= 4z_1 \sqrt{T_S} \alpha \beta \\ x_3 &= 2iz_1 d(\beta + \alpha T_S), & y_3 &= 2z_1 \beta^2, \\ x_4 &= 2iz_1 \sqrt{T_S} d e^r, & y_4 &= -2iz_1 d \alpha^{-1} \beta e^r, \\ x_5 &= \frac{z_1}{2}(T_S - 1)d^2 e^{2r}, & y_5 &= 2iz_1 \sqrt{T_S} d e^r, \\ z_1 &= [2(\beta^2 - \alpha^2 T_S)]^{-1} & y_6 &= \frac{-z_1}{2\alpha^2} d^2 e^{2r}, \\ z_2 &= 2z_1 \alpha^2 (1 - T_S) \end{aligned} \quad (9)$$

with  $\alpha = \sinh r$  and  $\beta = \cosh r$ .

**Probability of  $k$ -photon detection:** We evaluate the probability of  $k$ -photon subtraction from Eq. (8) as

$$P_{PS}^{(k)} = \tilde{\chi}_{A_1 A'_2}^{(k)}(\Lambda_1, \Lambda_2) \Big|_{\substack{\tau_1=\sigma_1=0 \\ \tau_2=\sigma_2=0}} = 2z_1 z_2^k \exp(x_5) L_k(y_6). \quad (10)$$

**Covariance matrix of the  $k$ -PSTMSC state:** The normalized Wigner characteristic function of the  $k$ -PSTMSC state becomes

$$\chi_{A_1 A'_2}^{(k)}(\Lambda_1, \Lambda_2) = \left(P_{PS}^{(k)}\right)^{-1} \tilde{\chi}_{A_1 A'_2}^{(k)}(\Lambda_1, \Lambda_2). \quad (11)$$

The average of a symmetrically ordered operator can be calculated by differentiating the Wigner characteristic

function of the  $k$ -PSTMSC state with respect to  $\tau$  and  $\sigma$  parameters as follows:

$$\langle \hat{q}_1^{r_1} \hat{p}_1^{s_1} \hat{q}_2^{r_2} \hat{p}_2^{s_2} \rangle = \widehat{F} \chi_{A_1 A'_2}^{(k)}(\tau_1, \sigma_1, \tau_2, \sigma_2), \quad (12)$$

where

$$\begin{aligned} \widehat{F} &= \left(\frac{1}{i}\right)^{r_1+r_2} \left(\frac{1}{-i}\right)^{s_1+s_2} \frac{\partial^{r_1+s_1}}{\partial \sigma_1^{r_1} \partial \tau_1^{s_1}} \\ &\times \frac{\partial^{r_2+s_2}}{\partial \sigma_2^{r_2} \partial \tau_2^{s_2}} \left\{ \bullet \right\}_{\substack{\tau_1=\sigma_1=0 \\ \tau_2=\sigma_2=0}}, \end{aligned} \quad (13)$$

and  $\left\{ \bullet \right\}$  represents Weyl ordering. We can choose the values of  $r_1$ ,  $s_1$ ,  $r_2$ ,  $s_2$  in Eq. (12) to yield all the elements of the covariance matrix. Here we provide the calculated expressions for different moments occurring in the covariance matrix:

$$\langle \hat{q}_1 \rangle = -i \left( x_3 - y_4 \frac{L_{k-1}^1(y_6)}{L_k(y_6)} \right), \quad (14)$$

$$\langle \hat{q}_2 \rangle = -i \left( x_4 - y_5 \frac{L_{k-1}^1(y_6)}{L_k(y_6)} \right), \quad (15)$$

$$\begin{aligned} \langle \hat{q}_1^2 \rangle &= - (x_3^2 + 2x_1) + 2(x_3 y_4 + y_1) \frac{L_{k-1}^1(y_6)}{L_k(y_6)} \\ &\quad - y_4^2 \frac{L_{k-2}^2(y_6)}{L_k(y_6)}, \end{aligned} \quad (16)$$

$$\begin{aligned} \langle \hat{q}_2^2 \rangle &= - (x_4^2 + 2x_1) + 2(x_4 y_5 + y_2) \frac{L_{k-1}^1(y_6)}{L_k(y_6)} \\ &\quad - y_5^2 \left( \frac{L_{k-2}^2(y_6)}{L_k(y_6)} \right), \end{aligned} \quad (17)$$

$$\langle \hat{p}_1^2 \rangle = -2x_1 + 2y_1 \frac{L_{k-1}^1(y_6)}{L_k(y_6)}, \quad (18)$$

$$\langle \hat{p}_2^2 \rangle = -2x_1 + 2y_2 \frac{L_{k-1}^1(y_6)}{L_k(y_6)}, \quad (19)$$

$$\begin{aligned} \langle \hat{q}_1 \hat{q}_2 \rangle &= - (x_2 + x_3 x_4) + (x_4 y_4 + x_3 y_5 + y_3) \frac{L_{k-1}^1(y_6)}{L_k(y_6)} \\ &\quad - y_4 y_5 \frac{L_{k-2}^2(y_6)}{L_k(y_6)}, \end{aligned} \quad (20)$$

$$\langle \hat{p}_1 \hat{p}_2 \rangle = x_2 - y_3 \frac{L_{k-1}^1(y_6)}{L_k(y_6)}, \quad (21)$$

$$\langle \hat{p}_1 \rangle = \langle \hat{p}_2 \rangle = \langle \hat{q}_1 \hat{p}_2 \rangle = \langle \hat{p}_1 \hat{q}_2 \rangle = \langle \hat{q}_1 \hat{p}_1 \rangle = \langle \hat{q}_2 \hat{p}_2 \rangle = 0. \quad (22)$$

Using these moments, the covariance matrix takes the following form:

$$\Sigma_{A_1 A'_2} = \begin{pmatrix} V_A^q & 0 & V_C^q & 0 \\ 0 & V_A^p & 0 & V_C^p \\ V_C^q & 0 & V_B^q & 0 \\ 0 & V_C^p & 0 & V_B^p \end{pmatrix}, \quad (23)$$

where  $(\Sigma_{A_1 A'_2})_{ij} = \frac{1}{2} \langle \{\hat{\xi}_i, \hat{\xi}_j\} \rangle - \langle \hat{\xi}_i \rangle \langle \hat{\xi}_j \rangle$ .

### B. PSTMSC state based CV-MDI-QKD protocol

In the current work, we consider PSTMSC state as resource state for CV-MDI-QKD. The schematic of the CV-MDI-QKD protocol is depicted in Fig. 2. The main steps of the protocol are described as follows:

**Step 1:** Alice starts with a TMSV state in modes  $A_1$  and  $A_2$  with variance  $V_A = \cosh(2r)$ .

**Step 2:** Alice sends one of her modes,  $A_2$ , to Fred, who performs a photon subtraction. The photon subtracted mode  $A'_2$  is then sent to Charlie through a quantum channel of length  $L_{AC}$ .

**Step 3:** Bob generates a TMSV state with the two modes denoted by  $B_1, B_2$  and variance  $V_B = V_A = V$ . He sends the mode  $B_2$  to Charlie through another quantum channel of length  $L_{BC}$ .

**Step 4:** Charlie interferes the two modes  $A'_2$  and  $B_2$ , obtained from Alice and Bob respectively, using a beam splitter, and the output modes are labeled  $C$  and  $D$ . He then employs homodyne measurements of quadrature  $\hat{q}$  on mode  $C$  and of quadrature  $\hat{p}$  on mode  $D$  to obtain outcomes  $\{Q_C, P_D\}$ . These outcomes are then publicly announced by Charlie.

**Step 5:** Based on these outcomes, Bob performs a displacement operation  $\hat{D}(g(Q_C + iP_D))$ , where  $g$  is the gain factor, on his retained mode  $B_1$  to obtain the transformed mode  $B'_1$ . This operation completes the entanglement swapping process, and the modes  $A_1$  and  $B'_1$  thus obtained are entangled. Alice and Bob implement heterodyne measurements on their retained modes to obtain outcomes  $\{Q_A, P_A\}$  and  $\{Q_B, P_B\}$  respectively. These outcomes are correlated with each other.

**Step 6:** Finally, Alice and Bob employ classical data post-processing, *i.e.*, information reconciliation (reverse reconciliation) and privacy amplification to distil the secret key.

We note that the analysis for the TMSV and PSTMSV states can be obtained as a special case of the PSTMSC state as detailed in next subsection.

### C. Security analysis and equivalent one-way CV-QKD

The CV-MDI-QKD protocol, as shown in Fig. 2, uses two quantum channels, one each for transmission of Alice's and Bob's modes to Charlie, and one classical channel, for classical communication. We assume the two

quantum channels to be non-interacting. With this assumption, one-mode entangling cloner collective attacks [21] on each of the two channels by Eve are possible, while the most general forms of eavesdropping include two-mode correlated attacks [21, 60].

In the CV-MDI-QKD protocol described in Fig. 2, all of Bob's operations can be assumed to be untrusted, except his heterodyne measurements. This lets us convert the protocol into an equivalent one-way CV-QKD protocol with heterodyne detection (Fig. 3) [22, 61, 62]. We note that by calculating the SKR for the equivalent one-way protocol, we obtain a lower bound on the SKR that we would have obtained using the original protocol. Despite this, we use the one-way protocol to calculate the SKR because of convenience in calculations [63].

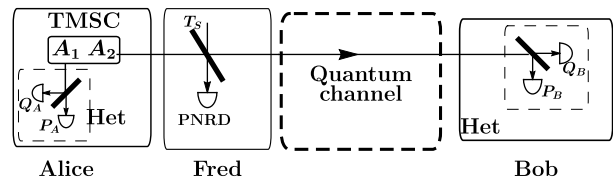


FIG. 3. Schematic of the PSTMSC state based one-way equivalent CV-MDI-QKD protocol.

In the one-way CV-QKD protocol, the total transmission distance from Alice to Bob is  $L_{AB} = L_{AC} + L_{BC}$ , where  $L_{AC}$  and  $L_{BC}$  are the transmission distances between Alice to Charlie and Bob to Charlie, which we shall express in kilometer (km). Usually, optical fiber networks are employed as channels for information transfer. The overall loss in the optical fiber between Alice to Charlie for a length  $L_{AC}$  is quantified as  $lL_{AC}$ , where  $l$  is the attenuation factor in decibels per kilometer (dB/km) [64]. For this work, we consider  $l = 0.2$  dB/km [65]. The transmissivity of the corresponding channel is related to its length via the relation  $T_A = 10^{-l \frac{L_{AC}}{10}}$ . Similarly, the transmissivity for the channel from Bob to Charlie is  $T_B = 10^{-l \frac{L_{BC}}{10}}$ .

We will be studying the following two cases in this article:

**Symmetric:** Charlie is considered to be exactly midway between Alice and Bob, so  $L_{AC} = L_{BC}$ . The total transmission distance  $L = 2L_{AC}$  with  $T_A = T_B$ .

**Extreme asymmetric:** Charlie is considered to be at the same position as Bob, so  $L_{BC} = 0$ . The total transmission distance  $L = L_{AC} = L_{AB}$  with  $T_B = 1$ .

The added noise in a quantum channel is defined as

$$\chi_{channel} = \frac{1-T}{T} + \varepsilon^{th}, \quad (24)$$

where  $T$  is a normalized parameter for transmissivity and  $\varepsilon^{th}$  is the thermal excess noise from the one-way protocol.  $T$  is defined in terms of  $T_A$  as

$$T = \frac{g^2}{2} T_A, \quad (25)$$

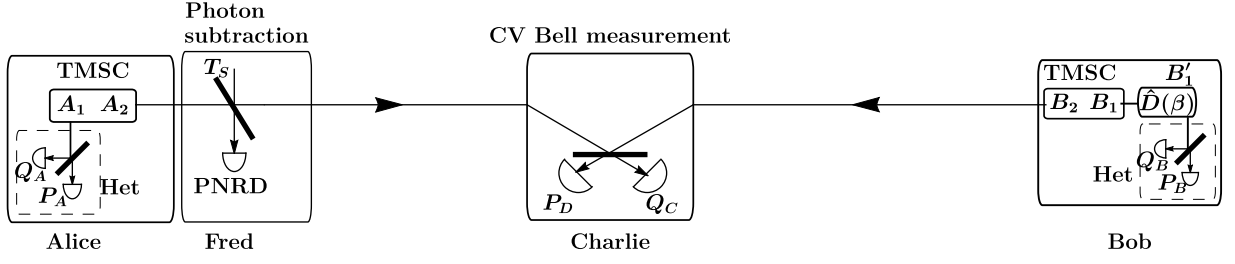


FIG. 2. Schematic of PSTMSC state based CV-MDI-QKD protocol. Alice and Bob start with a TMSC state. Alice sends one of her modes to Fred, an untrusted party, for photon subtraction. The mode is subsequently sent to Charlie, another untrusted party, who then mixes it with the mode received from Bob using a balanced (50-50) beam splitter. He then executes homodyne measurement on the output modes and publicly announces the result. Bob then performs a displacement operation leading to the entanglement of the modes that were retained by Alice and Bob. They then perform heterodyne measurements on their respective modes.

where  $g$  is the gain of the displacement operation employed by Bob. The thermal excess noise is given by [39]

$$\varepsilon^{th} = \frac{T_B}{T_A} (\varepsilon_B^{th} - 2) + \varepsilon_A^{th} + \frac{2}{T_A}, \quad (26)$$

where  $\varepsilon_A^{th}$  and  $\varepsilon_B^{th}$  are the thermal excess noises in the quantum channels from Alice and Bob to Charlie respectively. For  $\varepsilon^{th}$  in Eq. (26) to be minimum, the gain is

$$g = \sqrt{\frac{2(V_A - 1)}{T_B(V_A + 1)}}. \quad (27)$$

The detectors used by Charlie for performing homodyne detection during entanglement swapping are assumed to be imperfect with excess noise given as

$$\chi_C = \frac{v_{el} + 1 - \eta}{\eta}, \quad (28)$$

where,  $v_{el}$  is the electronic noise of the detector with quantum efficiency  $\eta$ . The total noise added that is to be considered for the entire setup is then

$$\chi_{total} = \chi_{channel} + \frac{2\chi_C}{T_A}. \quad (29)$$

In this article, we have considered both cases of Charlie performing perfect ( $\chi_C = 0$ ) and imperfect homodyne detection. The latter is studied exclusively in Sec. III D.

The SKR of the protocol described in Sec. II with channel parameters as given above is

$$K = P_{PS}^{(k)} (\mathcal{R}I_{AB} - \chi_{BE}), \quad (30)$$

where  $I_{AB}$  is the mutual information between Alice and Bob,  $\chi_{BE}$  is the Holevo bound between Bob and Eve,  $\mathcal{R}$  is the reconciliation efficiency. We utilize the covariance matrix derived in Eq. (23) for the calculation of SKR for the non-Gaussian PSTMSC state, which provides a lower bound of the SKR according to the optimality of Gaussian attacks [66].

We start with the calculation of the mutual information. The covariance matrix of the state  $\hat{\rho}_{A_1 B'_1}$ , obtained

after Bob operates the displacement operator  $\hat{D}$  on his retained mode  $B'_1$  is given by

$$\Sigma_{A_1 B'_1} = \begin{pmatrix} V_A^q & 0 & \sqrt{T}V_C^q & 0 \\ 0 & V_A^p & 0 & \sqrt{T}V_C^p \\ \sqrt{T}V_C^q & 0 & T(V_B^q + \chi_{total}) & 0 \\ 0 & \sqrt{T}V_C^p & 0 & T(V_B^p + \chi_{total}) \end{pmatrix},$$

$$= \begin{pmatrix} \delta_1 & 0 & \kappa_1 & 0 \\ 0 & \delta_2 & 0 & \kappa_2 \\ \kappa_1 & 0 & \mu_1 & 0 \\ 0 & \kappa_2 & 0 & \mu_2 \end{pmatrix} = \begin{pmatrix} \Sigma_{A_1} & \Sigma_C \\ \Sigma_C & \Sigma_{B'_1} \end{pmatrix}. \quad (31)$$

The mutual information between Alice and Bob is given as [67]

$$I_{AB} = \frac{1}{2} \log_2 \left( \frac{\Sigma_{A_1}^q + 1}{\Sigma_{A_1|B'_1}^q + 1} \right) + \frac{1}{2} \log_2 \left( \frac{\Sigma_{A_1}^p + 1}{\Sigma_{A_1|B'_1}^p + 1} \right), \quad (32)$$

where  $\Sigma_{A_1|B'_1}$  is the conditional variance of the outcome of Alice depending on Bob's heterodyne measurement results and can be evaluated from

$$\Sigma_{A_1|B'_1} = \Sigma_{A_1} - \Sigma_C (\Sigma_{B'_1} + \mathbb{1}_2)^{-1} (\Sigma_C)^T,$$

$$= \begin{pmatrix} \delta_1 - \frac{\kappa_1^2}{\mu_1 + 1} & 0 \\ 0 & \delta_2 - \frac{\kappa_2^2}{\mu_2 + 1} \end{pmatrix}. \quad (33)$$

To calculate the Holevo bound, we assume that Eve holds a purification of the state  $\hat{\rho}_{A_1 B'_1 EF}$  having access to Fred's mode. The Holevo bound between Bob and Eve is

$$\chi_{BE} = S(\hat{\rho}_{A_1 B'_1}) - S(\hat{\rho}_{A_1|B'_1}), \quad (34)$$

where  $S(\hat{\rho})$  is the von-Neumann entropy for the state  $\hat{\rho}$  and is given by

$$S(\hat{\rho}) = \sum_i g(\lambda_i), \quad (35)$$

where,

$$g(\lambda) = \frac{\lambda + 1}{2} \log_2 \left( \frac{\lambda + 1}{2} \right) - \frac{\lambda - 1}{2} \log_2 \left( \frac{\lambda - 1}{2} \right), \quad (36)$$

and  $\lambda_i$  are the symplectic eigenvalues of the corresponding matrices.  $S(\hat{\rho}_{A_1 B_1'})$  is calculated using the symplectic eigenvalues of the matrix in Eq. (31) which evaluate as

$$\lambda_{1,2} = \frac{1}{\sqrt{2}} \left[ X \pm \sqrt{X^2 - 4Y} \right]^{1/2}, \quad (37)$$

with  $X = \delta_1 \delta_2 + \mu_1 \mu_2 + 2\kappa_1 \kappa_2$  and  $Y = (\delta_1 \mu_1 - \kappa_1^2)(\delta_2 \mu_2 - \kappa_2^2)$ , while  $S(\hat{\rho}_{A_1 | B_1'})$  is calculated using the symplectic eigenvalue of the matrix in Eq. (33) which evaluates as

$$\lambda_3 = \sqrt{\left( \delta_1 - \frac{\kappa_1^2}{\mu_1 + 1} \right) \left( \delta_2 - \frac{\kappa_2^2}{\mu_2 + 1} \right)}. \quad (38)$$

Using these expressions, secret key rate (30) can be readily evaluated.

**Special cases:** On setting  $d = 0$ , we obtain the SKR for the PSTMSV state. Further, in the unit transmissivity limit  $T_S \rightarrow 1$  with  $d = 0$  and  $k = 0$ , we obtain the SKR for TMSV state.

### III. OPTIMIZATION OF STATE PARAMETERS

After describing the CV-MDI-QKD protocol in detail, we now proceed to optimize the state parameters in order to maximize the SKR. We note that, for PSTMSC states, the state parameters are variance, displacement, and transmissivity. Similarly, for the PSTMSV state, which is obtained when displacement is zero, the state parameters reduce to only variance and transmissivity. We consider two different optimization scenarios for the SKR: (i) optimization of SKR with respect to displacement  $d$  and transmissivity  $T_S$  at a fixed variance, (ii) optimization of SKR with respect to all the state parameters  $V$ ,  $d$ , and  $T_S$ .

#### A. Optimization of $d$ and $T_S$

We consider the optimization of displacement and transmissivity, at a fixed variance, in order to maximize the SKR for the PSTMSC resource state. The displacement range has been set to  $d \in (0, 5)$ , as increasing beyond it only improves the key rate slightly, but the average number of photons increases significantly which requires a high-powered source for preparing the resource state. For the PSTMSV resource state, we need to only optimize with respect to transmissivity, at a fixed variance, to maximize the SKR. TMSV state with a maximum squeezing of 15 dB has been achieved [68], which is equivalent to a squeezing of  $r = 1.73$  or a variance of  $V = \cosh 2r = 15.83$ . We, therefore, optimize the above parameters at three fixed variance values ( $V = 5, 10, \text{ and } 15$ ) to maximize the SKR:

$$\begin{aligned} \max_{d, T_S} \quad & K(V, d, T_S) \\ \text{s.t.} \quad & 0 \leq d \leq 5, \\ & 0 \leq T_S \leq 1. \end{aligned} \quad (39)$$

We note that the optimization of state parameters is performed for each value of transmission distance.

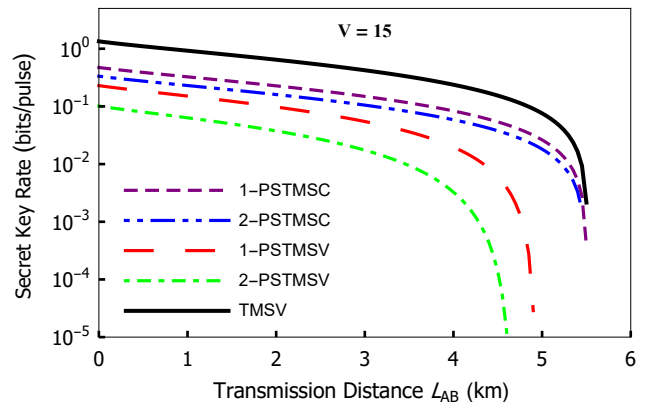


FIG. 4. [Color online] Secret key rate (SKR) as a function of transmission distance for fixed variance ( $V = 15$ ) in the symmetric case ( $L_{AB} = 2L_{AC} = 2L_{BC}$ ) using perfect homodyne detectors ( $\eta = 1, \nu_{el} = 0$ ). The SKR has been optimized with respect to displacement and transmissivity. Here, reconciliation efficiency  $\mathcal{R} = 0.96$ , and excess noise  $\epsilon_A^{\text{th}} = \epsilon_B^{\text{th}} = 0.002$ .

We first consider the symmetric case, *i.e.*, Charlie is based between Alice and Bob. It has been shown in earlier works that the symmetric case yields an extremely low value of maximum transmission distance [21, 22]; therefore, we analyze this case briefly for only  $V = 15$ .

We plot the SKR as a function of transmission distance for  $V = 15$  in Fig. 4. As we have mentioned earlier, for the symmetric case, the maximum transmission distance of TMSV falls around 5.5 km. The TMSV, 1-PSTMSC, and 2-PSTMSC states yield the same maximum transmission distance. However, the SKR for the 1-PSTMSC and 2-PSTMSC states is less as compared to the TMSV state SKR. We also observe that 1-PSTMSV and 2-PSTMSV states yield smaller maximum transmission distance and SKR as compared to all the aforementioned states.

We now proceed to analyze the extreme asymmetric case, where Charlie is located close to Bob, *i.e.*,  $L_{BC} = 0$  km. Figure 5 shows the plot of SKR as a function of transmission distance for three different fixed variances:  $V = 5, 10, \text{ and } 15$ . The results show that while the photon-subtracted states yield a constant maximum transmission distance with changing variance; for the TMSV state, the maximum transmission distance decreases with increasing variance. This indicates a positive role played by photon subtraction. We now stress on the role of displacement through two specific points: (i) The maximum transmission distance and the SKR achieved by the 1-PSTMSC and 2-PSTMSC states outperform the respective values of both the PSTMSV states (ii) In addition, we notice that, unlike the PSTMSV states, the maximum transmission distance achieved by 1-PSTMSC and 2-PSTMSC states is almost same, which suggests that displacement might be capable of maintaining the same maximum transmission distance for multiphoton

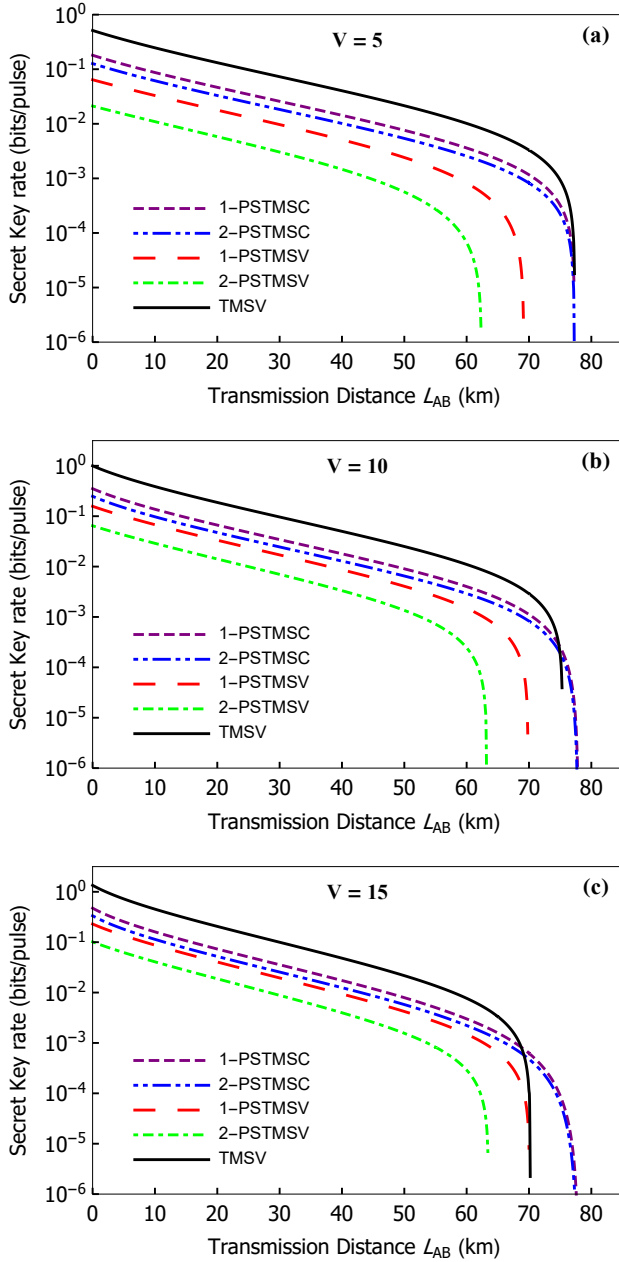


FIG. 5. [Color online] Secret key rate (SKR) as a function of transmission distance for fixed variances: (a)  $V = 5$ , (b)  $V = 10$ , (c)  $V = 15$ , in the extreme asymmetric case ( $L_{BC} = 0$  km) using perfect homodyne detectors ( $\eta = 1, \nu_{el} = 0$ ). The SKR has been optimized with respect to displacement and transmissivity. Here, reconciliation efficiency  $\mathcal{R} = 0.96$ , and excess noise  $\epsilon_A^{\text{th}} = \epsilon_B^{\text{th}} = 0.002$ .

subtracted states. This interesting fact is explored in the next section and exploited for a novel protocol that ensures maximum usage of resources.

For variance  $V = 5$ , the maximum transmission distance of 1-PSTMSC and 2-PSTMSC states is almost the same as the TMSV state; however, the secret key rate for the TMSV state is higher as compared to 1-PSTMSC and 2-PSTMSC states. Both 1-PSTMSV

and 2-PSTMSV states underperform in terms of SKR and maximum transmission distance as compared to the aforementioned states. For variance  $V = 10$  and  $V = 15$ , the maximum transmission distance of 1-PSTMSC and 2-PSTMSC states is higher compared to the TMSV state, but with a slight decrease in the SKR. On comparison with the results of earlier works, the optimization of parameters not only leads to the enhancement of maximum transmission distance, but also a substantial improvement in SKR.

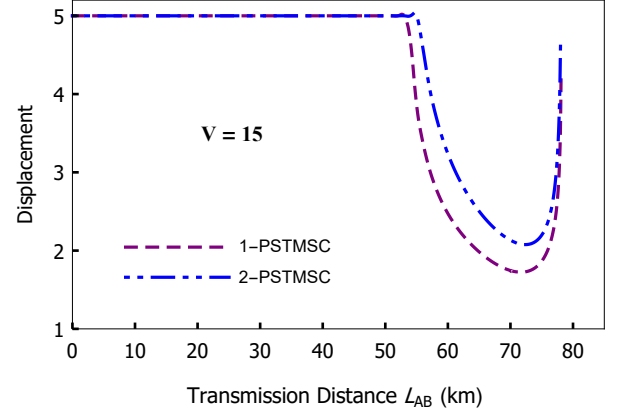


FIG. 6. [Color online] Optimal displacement for the maximal secret key rate (SKR) as a function of transmission distance for a fixed variance ( $V = 15$ ) in the extreme asymmetric case using perfect homodyne detectors ( $\eta = 1, \nu_{el} = 0$ ). Here, reconciliation efficiency  $\mathcal{R} = 0.96$ , and excess noise  $\epsilon_A^{\text{th}} = \epsilon_B^{\text{th}} = 0.002$ .

In Fig 6, we show the optimal displacement as a function of transmission distance, which maximizes the SKR for 1-PSTMSC and 2-PSTMSC states for  $V = 15$  (Fig 5(c)). The displacement remains equal to 5 for transmission distances below  $L_{AB} \approx 50$  km, after which it starts to decrease. As the transmission distance is increased, it attains a minima and then has a steep rise. We notice that the displacement required to obtain maximal SKR for a 1-PSTMSC state is lower than the 2-PSTMSC state.

We plot the probability of successful photon subtraction as a function of variance in Fig. 7, where the optimal displacement and transmissivity which maximize the SKR for  $V = 15$  (Fig 5(c)) and a transmission distance of  $L_{AB} = 60$  km have been taken. The magnitude of probability can also be interpreted as a measure of resource usage. At  $V = 15$ , the probabilities for 1-PSTMSC, 2-PSTMSC, 1-PSTMSV and 2-PSTMSV states are 0.33, 0.22, 0.23, and 0.15, respectively. Therefore, maximum resource usage occurs for the 1-PSTMSC state.

## B. Post selection of photon subtracted state

As explicit from Fig. 5, the maximum transmission distance of 2-PSTMSC is the same as 1-PSTMSC. We

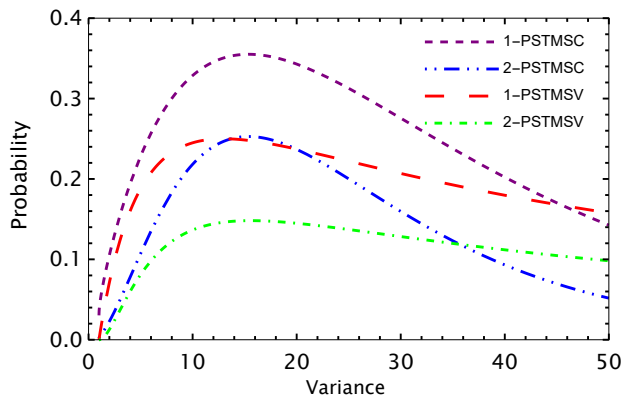


FIG. 7. [Color online] Probability of successful photon subtraction as a function of variance. Optimal displacement and transmissivity for the extreme asymmetric case using perfect homodyne detectors ( $\eta = 1, \nu_{el} = 0$ ) at transmission distance of  $L_{AB} = 60$  km have been considered.

explicitly provide the maximum transmission distances of up to 4-PSTMSC and 4-PSTMSV states in table I. We observe that all the  $k$ -PSTMSC states have almost the same maximum transmission distances, while for PSTMSV states, the maximum transmission distance decreases as  $k$  is increased.

TABLE I. Maximum transmission distance  $d_{\max}$  for  $k$ -PSTMSC and  $k$ -PSTMSV states.

State	$d_{\max}$ (in km)	State	$d_{\max}$ (in km)
1-PSTMSV	69.9	1-PSTMSC	76.8
2-PSTMSV	63.3	2-PSTMSC	76.5
3-PSTMSV	57.3	3-PSTMSC	76.3
4-PSTMSV	51.8	4-PSTMSC	76.1

Therefore, we can envisage a new QKD protocol, where we can use different photon subtracted TMSV states for key generation. To this end, Fred uses a PNRD, which can detect up to  $N$  photons. The positive operator valued measure (POVM) of such a PNRD can be written as

$$\left\{ \Pi_0, \Pi_1, \dots, \Pi_k, \dots, \Pi_N, \mathbb{1} - \sum_{k=0}^N \Pi_k \right\}, \quad \Pi_k = |k\rangle\langle k|. \quad (40)$$

On detection of  $k$  photons, Fred announces publicly that  $k$  photons have been subtracted. This information is used to construct an effective information channel for each  $k$  [69]. Further steps in the QKD protocol including classical post-processing on each of these effective information channel is done separately [70]. Denoting the SKR for the  $k$ -PSTMSC state by  $K(\hat{\rho}^{(k)})$ , the average SKR

over different information channels can be written as [2]

$$K_{\text{avg}} = \sum_{k=1}^N K(\hat{\rho}^{(k)}). \quad (41)$$

We note that we have excluded zero-photon catalyzed TMSV state ( $k = 0$ ) from the calculation of  $K_{\text{avg}}$ . Further, we have restricted the range of  $k$  to be  $k \in (1, 4)$ , *i.e.*,  $N_{\max} = 4$ .

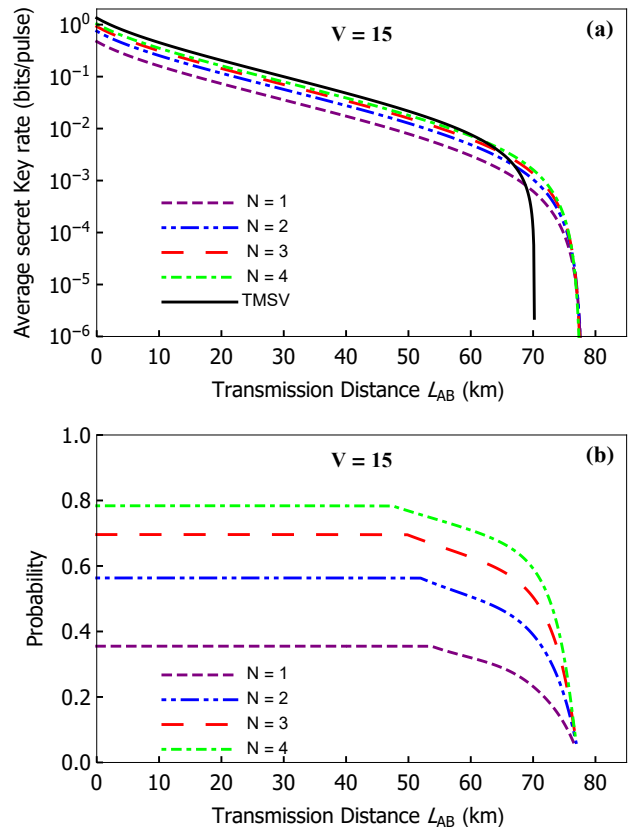


FIG. 8. [Color online] (a) Average secret key rate (SKR) as a function of transmission distance for fixed variance  $V = 15$ , in the extreme asymmetric case ( $L_{BC} = 0$  km) using perfect homodyne detectors ( $\eta = 1, \nu_{el} = 0$ ).  $N$  represents the contribution in the SKR obtained from 1-PSTMSC, 2-PSTMSC, ...,  $N$ -PSTMSC states. The SKR has been optimized with respect to displacement and transmissivity. Here, reconciliation efficiency  $\mathcal{R} = 0.96$ , and excess noise  $\epsilon_A^{\text{th}} = \epsilon_B^{\text{th}} = 0.002$ . (b) Probability as a function of transmission distance. Probability has been calculated for optimum displacement and transmissivity at every transmission distance.

Figure 8(a) shows the plot of the SKR as a function of transmission distance for  $N = 1, 2, 3$ , and 4. We observe that while there is no enhancement in maximum transmission distance, the SKR does show an improvement. Further, as the value of  $N$  is increased, the SKR also increases. We plot the total probability  $P_{\text{total}} = \sum_{k=1}^N P(\hat{\rho}^{(k)})$  as a function of the transmission distance in Fig. 8(b) for  $N = 1, 2, 3$ , and 4. The total probability reaches up to a maximum of 0.36, 0.56, 0.69,



and 0.78 for  $N = 1, 2, 3$ , and 4, respectively. Thus, we see that as  $N$  is increased, the total probability increases. As mentioned earlier, the probability of photon subtraction is a measure of the resource state utilization per trial. The enhancement of the total probability indicates an efficient utilization of the resource state providing an enhancement in the SKR in our new scheme.

### C. Optimization of $V$ , $d$ and $T_S$

In this subsection, we optimize the variance, displacement, and transmissivity for various states in order to maximize the SKR:

$$\begin{aligned} \max_{V, d, T_S} \quad & K(V, d, T_S) \\ \text{s.t.} \quad & 1 \leq V \leq 15, \\ & 0 \leq d \leq 5, \\ & 0 \leq T_S \leq 1. \end{aligned} \quad (42)$$

We plot the SKR as a function of transmission distance in the extreme asymmetric case using perfect homodyne detectors in Fig. 9(a). We observe that the maximum transmission distance of TMSV and PSTMSC states are the same; however, the SKR for the TMSV state is higher as compared to PSTMSC states. The PSTMSV states underperform in terms of both the SKR and the maximum transmission distance as compared to the aforementioned states. Therefore, photon subtraction operations do not enhance the SKR or the maximum transmission distance.

The optimized variance as a function of transmission distance is shown in Fig. 9(b). We note that the SKR is maximized at the maximum allowed variance  $V = 15$  up to a transmission distance  $L_{AB} \approx 30$  km for TMSV and PSTMSC states. The optimal variance tends to decrease as the transmission distance is increased and reaches a minimum value of  $V \approx 6$  at the maximum transmission distance. For the 1-PSTMSV states, the optimal variance remains equal to 15 for larger transmission distances. The optimal variance decreases, attains minima, and then starts increasing as the transmission distance is increased further. For the 2-PSTMSV states, the optimal variance remains at  $V = 15$  for all transmission distances.

To conclude this section, we find that neither PSTMSC nor PSTMSV state provides any advantage over the TMSV state when the optimization is performed with respect to all state parameters. We obtain enhanced performance at fixed high variance but as states with small variance are easy to prepare, it is better to work with TMSV or TMSV state.

### D. Imperfect detectors

We now consider the case of imperfect homodyne detectors at fixed variance  $V = 15$ . In Fig. 10(a), we plot

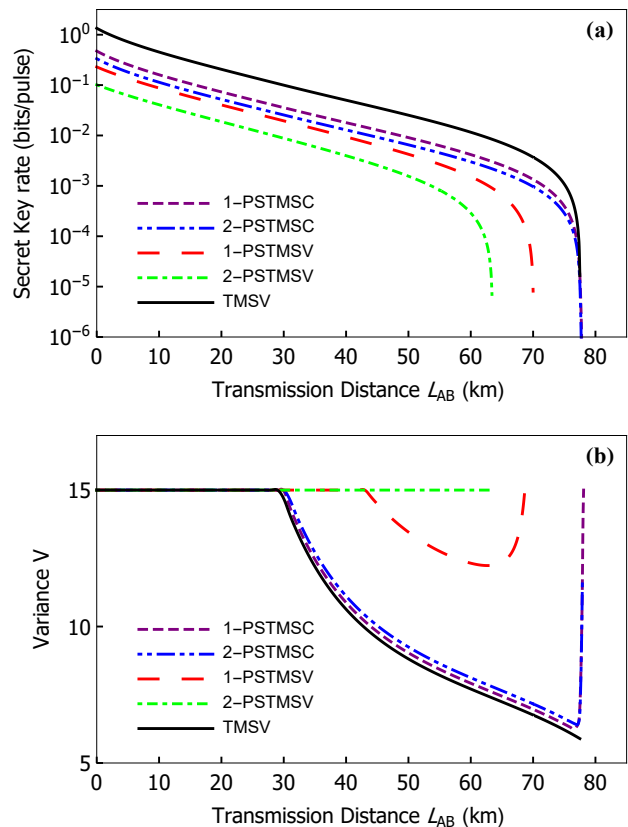


FIG. 9. [Color online] (a) Secret key rate (SKR) as a function of transmission distance in the extreme asymmetric case using perfect homodyne detectors ( $\eta = 1, \nu_{el} = 0$ ). The SKR has been optimized with respect to variance, displacement, and transmissivity. (b) Optimal variance maximizing the SKR as a function of transmission distance. Here, reconciliation efficiency  $\mathcal{R} = 0.96$ , and excess noise  $\epsilon_A^{\text{th}} = \epsilon_B^{\text{th}} = 0.002$ .

the SKR, optimized with respect to displacement and transmissivity, as a function of transmission distance in the extreme asymmetric case. The efficiency and the electronic noise corresponding to Charlie's homodyne detectors are set as  $\eta = 0.995, \nu_{el} = 0.01$ . We observe that the transmission distance reduces significantly from  $L_{AB} = 80$  km (Fig. 5(c)) to  $L_{AB} = 30$  km. Further, the difference in the maximum transmission distance between TMSV and 1-PSTMSC state reduces from 8 km (Fig. 5(c)) to 1 km. Furthermore, the maximum transmission distance for the PSTMSV states is lower than the TMSV state.

We plot the SKR as a function of the efficiency of the homodyne detector in Fig. 10(b). We see that the TMSV state is most robust to detector noise, followed by the PSTMSC states. To provide numerical values, the TMSV and PSTMSC states can yield SKR up to a threshold detector efficiency of  $\eta = 0.953$ . Further, for the 1-PSTMSV and 2-PSTMSV states, the threshold efficiency increases to  $\eta = 0.962$  and  $\eta = 0.966$ , respectively.

In Fig. 11(a), we plot the SKR optimized with respect to variance, displacement, and transmissivity as a func-

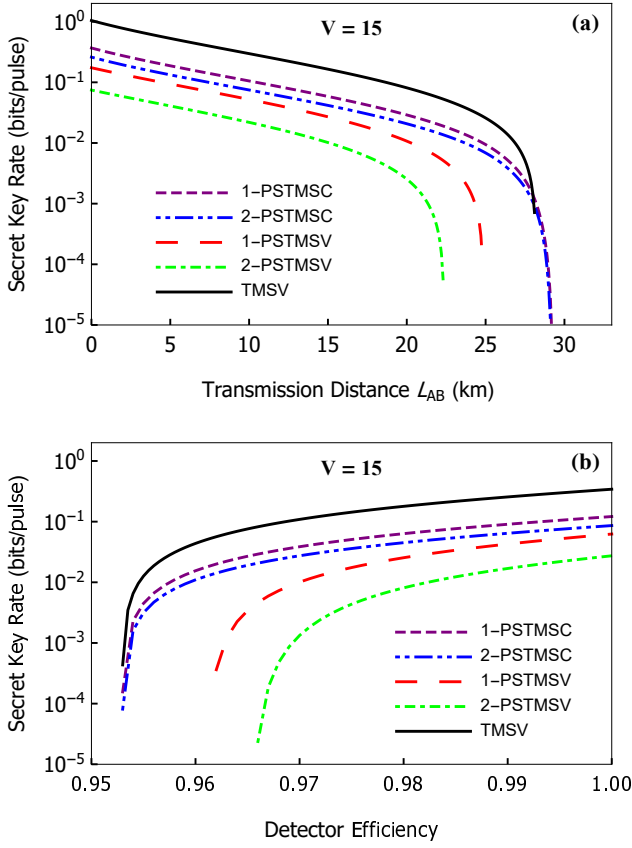


FIG. 10. [Color online] (a) Secret key rate (SKR) as a function of transmission distance for fixed variance ( $V = 15$ ) in the extreme asymmetric case using imperfect homodyne detectors ( $\eta = 0.995$ ,  $\nu_{el} = 0.01$ ). (b) Secret key rate (SKR) as a function of the efficiency of the homodyne detector. The SKR has been optimized with respect to displacement and transmissivity. Here, reconciliation efficiency  $\mathcal{R} = 0.96$ , and excess noise  $\epsilon_A^{\text{th}} = \epsilon_B^{\text{th}} = 0.002$ . The transmission distance has been fixed at 10 km.

tion of transmission distance for the extreme asymmetric case. We observe that the PSTMSC state outperforms the TMSV state in terms of maximum transmission distance by a very small margin but underperforms in terms of the SKR. On the other hand, the PSTMSV states have smaller transmission distances than the TMSV state.

The plot of the SKR as a function of the efficiency of the homodyne detector is shown in Fig. 11(b). It can be seen that the TMSV and PSTMSC states can yield an SKR up to a threshold detector efficiency of  $\eta \approx 0.954$ . Further, for the 1-PSTMSV and 2-PSTMSV states, the threshold efficiency increases to  $\eta = 0.962$  and  $\eta = 0.966$ , respectively.

#### IV. CONCLUSION

In this work, we critically examined the benefits of the PSTMSV and PSTMSC resource states in CV-MDI-QKD as claimed in Refs. [39, 40]. To this end, we de-

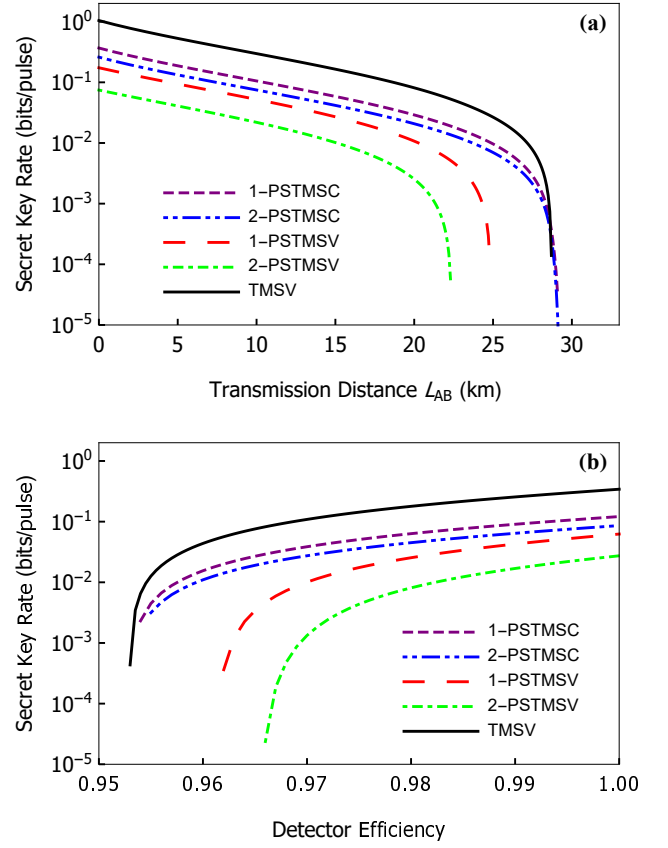


FIG. 11. [Color online] (a) Secret key rate (SKR) as a function of transmission distance in the extreme asymmetric case using imperfect homodyne detectors ( $\eta = 0.995$ ,  $\nu_{el} = 0.01$ ). (b) SKR as a function of the efficiency of the homodyne detector. The SKR has been optimized with respect to variance, displacement, and transmissivity. Here, reconciliation efficiency  $\mathcal{R} = 0.96$ , and excess noise  $\epsilon_A^{\text{th}} = \epsilon_B^{\text{th}} = 0.002$ . The transmission distance has been fixed at 10 km.

rive the Wigner characteristic function of the PSTMSC resource states, which is then used to derive its covariance matrix. In the first scenario, the evaluated SKR is maximized with respect to displacement and transmissivity for various fixed variances. This significantly improved the performance of PSTMSC states and established its superiority over the PSTMSV states in terms of both SKR and maximum transmission distance up to which secure QKD can be implemented. Although PSTMSV states are never superior when compared to TMSV states, PSTMSC states only offer an advantage over TMSV states under conditions of high variance.

In the second scenario, where we perform optimization of the SKR with respect to variance, displacement, and transmissivity, we find that the photon subtraction operation on Alice's side does not provide any benefits over the TMSV state. The optimal variance is relatively small at large transmission distances. Since preparing states with low variances is less challenging, our work conclusively establishes that performing PS operation by Alice

on TMSV and TMSC states is unessential, unlike the conclusion of earlier works for PSTMSV and PSTMSC state.

In this work, we have focused on photon subtraction only on Alice's side. It is essential to consider photon subtraction on Bob's side, as well as its advantage in other CV-QKD protocols [57–59] needs to be assessed. Our work shows that photon subtraction on Alice's side for CV-MDI-QKD is unessential and raises numerous questions regarding the utility of non-Gaussian operations in CV quantum information processing, which is currently pursued by a large community of researchers.

Photon subtraction has been shown to be useful in quantum teleportation [30–37] and quantum metrology [44–53]. The potential benefits of photon subtraction and other non-Gaussian operations such as photon catalysis [71, 72] and photon addition [73] in CV-QKD and other CV-QIP tasks demand a thorough examination.

We proposed a new protocol that maximizes resource utilization by exploiting the fact that multiphoton subtracted TMSC state yields the same maximum transmission distance as that of 1-PSTMSC. This protocol does not provide any improvements in the maximum transmission distance, but the SKR increases as compared to 1-PSTMSC resource state. It should be stressed that this protocol is effective at high variance.

We have also derived the Wigner characteristic function of the PSTMSC states, which can be helpful in studying nonclassicality [74–76], nonlocality [77, 78], and non-Gaussianity [79] as well as can be employed in various other QIP protocols such as entanglement swapping, quantum teleportation, and quantum metrology.

## ACKNOWLEDGEMENT

S.C. acknowledges the Prime Minister's Research Fellowship (PMRF) scheme, GoI, for financial support. A and C.K. acknowledge the financial support from **DST/ICPS/QuST/Theme-1/2019/General** Project number Q-68.

## Appendix A: Phase space formalism of CV systems and Wigner characteristic function for the PSTMSC state

In this section, we give a brief overview of CV systems and their description using Wigner characteristic functions. We then provide a detailed calculation of the Wigner characteristic function for PSTMSC states, the corresponding success probability, and the covariance matrix.

## 1. CV systems

An  $n$ -mode continuous variable quantum system can be represented via  $n$  pairs of Hermitian quadrature operators [13, 80–83]

$$\hat{\xi} = (\hat{\xi}_i) = (\hat{q}_1, \hat{p}_1, \dots, \hat{q}_n, \hat{p}_n)^T, \quad i = 1, 2, \dots, 2n. \quad (\text{A1})$$

The commutation relation between the quadrature operators can be succinctly expressed in shot noise units ( $\hbar=2$ ) as

$$[\hat{\xi}_i, \hat{\xi}_j] = 2i\Omega_{ij}, \quad (i, j = 1, 2, \dots, 2n), \quad (\text{A2})$$

where  $\Omega$  is given by

$$\Omega = \bigoplus_{k=1}^n \omega = \begin{pmatrix} \omega & & \\ & \ddots & \\ & & \omega \end{pmatrix}, \quad \omega = \begin{pmatrix} 0 & 1 \\ -1 & 0 \end{pmatrix}. \quad (\text{A3})$$

Alternatively, an  $n$ -mode continuous variable quantum system can also be represented via  $n$ -pairs of annihilation  $\hat{a}_i$  and creation operators  $\hat{a}_i^\dagger$  ( $i = 1, 2, \dots, n$ ). The operators  $\hat{a}_i$  and  $\hat{a}_i^\dagger$  are related via the quadrature operators as

$$\hat{a}_i = \frac{1}{2}(\hat{q}_i + i\hat{p}_i), \quad \hat{a}_i^\dagger = \frac{1}{2}(\hat{q}_i - i\hat{p}_i). \quad (\text{A4})$$

The displacement operator displacing the  $\hat{q}_i$  and  $\hat{p}_i$  quadratures in phase space by an amount  $q_i$  and  $p_i$ , respectively, is defined as

$$\hat{D}_i(q_i, p_i) = e^{i(p_i\hat{q}_i - q_i\hat{p}_i)}. \quad (\text{A5})$$

Symplectic transformations are the linear homogeneous transformations characterized by real  $2n \times 2n$  matrices  $S$ , and act on the quadrature operators as  $\hat{\xi}_i \rightarrow \hat{\xi}'_i = S_{ij}\hat{\xi}_j$ . Symplectic matrices satisfy the condition  $S\Omega S^T = \Omega$ , which can be obtained from the commutation relations (A2). We define below two important symplectic transformation which represent the beam splitter action and two-mode squeezer, which are relevant to this work.

**Beam splitter:** The action of a beam splitter on the quadrature operators  $\hat{\xi} = (\hat{q}_i, \hat{p}_i, \hat{q}_j, \hat{p}_j)^T$  of a two-mode system is defined through the following transformation matrix:

$$B_{ij}(T_S) = \begin{pmatrix} \sqrt{T_S} \mathbb{1} & \sqrt{1-T_S} \mathbb{1} \\ -\sqrt{1-T_S} \mathbb{1} & \sqrt{T_S} \mathbb{1} \end{pmatrix}, \quad (\text{A6})$$

where  $T_S$  is the beam splitter transmissivity.

The beam splitter acts on the quantum states of the two mode field via an infinite-dimensional unitary operator corresponding of the above action given by [80, 84, 85]

$$\mathcal{U}(B_{ij}(T_S)) = \exp[\theta(\hat{a}_i^\dagger \hat{a}_j - \hat{a}_i \hat{a}_j^\dagger)], \quad (\text{A7})$$

where  $\theta$  is related to the transmissivity via the relation  $T_S = \cos^2 \theta$ .

**Two mode squeezer:** It acts on the quadrature operators  $(\hat{q}_i, \hat{p}_i, \hat{q}_j, \hat{p}_j)^T$  through the matrix

$$S_{ij}(r) = \begin{pmatrix} \cosh r \mathbb{1} & \sinh r \mathbb{Z} \\ \sinh r \mathbb{Z} & \cosh r \mathbb{1} \end{pmatrix}, \quad (\text{A8})$$

where  $\mathbb{Z} = \text{diag}(1, -1)$ . The infinite-dimensional unitary operator for the two-mode squeezer acting on the Hilbert space is given by

$$\mathcal{U}(S_{ij}(r)) = \exp[r(\hat{a}_i^\dagger \hat{a}_j^\dagger - \hat{a}_i \hat{a}_j)]. \quad (\text{A9})$$

## 2. Wigner characteristic function

The Wigner characteristic function for a state of an  $n$ -mode quantum system represented by the density operator  $\hat{\rho}$  can be written as

$$\chi(\Lambda) = \text{Tr}[\hat{\rho} \exp(-i\Lambda^T \Omega \hat{\xi})], \quad (\text{A10})$$

where  $\hat{\xi} = (\hat{q}_1, \hat{p}_1, \dots, \hat{q}_n, \hat{p}_n)^T$ ,  $\Lambda = (\Lambda_1, \Lambda_2, \dots, \Lambda_n)^T$  with  $\Lambda_i = (\tau_i, \sigma_i)^T \in \mathcal{R}^2$ . Using the above equation, the Wigner characteristic function for a single mode Fock state  $|n\rangle$  evaluates to

$$\chi_{|n\rangle}(\tau, \sigma) = \exp\left[-\frac{\tau^2}{2} - \frac{\sigma^2}{2}\right] L_n(\tau^2 + \sigma^2), \quad (\text{A11})$$

where  $L_n(x)$  is the Laguerre polynomial.

First-order moments for an  $n$ -mode quantum system can be written as

$$\bar{\xi} = \langle \hat{\xi} \rangle = \text{Tr}[\hat{\rho} \hat{\xi}], \quad (\text{A12})$$

which we call the displacement vector. Similarly, second-order moments can be conveniently arranged in the form of a real symmetric  $2n \times 2n$  matrix, known as the covariance matrix given by

$$V = (V_{ij}) = \frac{1}{2} \langle \{\Delta \hat{\xi}_i, \Delta \hat{\xi}_j\} \rangle, \quad (\text{A13})$$

where  $\Delta \hat{\xi}_i = \hat{\xi}_i - \langle \hat{\xi}_i \rangle$ , and  $\{, \}$  denotes the anti-commutator operation.

Gaussian states, which play a very important role in quantum optics and various QIP schemes are defined as states with a Gaussian Wigner function or Gaussian Wigner characteristic function. Such states are completely specified by their displacement vectors and covariance matrices. For a Gaussian state with displacement vector  $\bar{\xi}$  and covariance matrix  $V$  the Wigner characteristic function takes a simple form [13, 86]:

$$\chi(\Lambda) = \exp\left[-\frac{1}{2} \Lambda^T (\Omega V \Omega^T) \Lambda - i(\Omega \bar{\xi})^T \Lambda\right]. \quad (\text{A14})$$

Therefore, the Wigner characteristic function of a single mode coherent state with displacement  $\bar{\xi} = (d_q, d_p)^T$  evaluates to

$$\chi_{\text{coh}}(\Lambda) = \exp\left[-\frac{1}{2}(\tau^2 + \sigma^2) - i(\tau d_p - \sigma d_q)\right]. \quad (\text{A15})$$

Given a symplectic transformation  $S$  and the associated infinite dimensional unitary representation  $\mathcal{U}(S)$ , the transformation of the density operator is given by  $\hat{\rho} \rightarrow \mathcal{U}(S)\hat{\rho}\mathcal{U}(S)^\dagger$ . Similarly, the displacement vector, the covariance matrix, and the Wigner characteristic function transform as by [13, 80, 86]

$$\bar{\xi} \rightarrow S\bar{\xi}, \quad V \rightarrow SVS^T, \quad \text{and } \chi(\Lambda) \rightarrow \chi(S^{-1}\Lambda). \quad (\text{A16})$$

- 
- [1] N. Gisin, G. Ribordy, W. Tittel, and H. Zbinden, Quantum cryptography, *Rev. Mod. Phys.* **74**, 145 (2002).
- [2] V. Scarani, H. Bechmann-Pasquinucci, N. J. Cerf, M. Dušek, N. Lütkenhaus, and M. Peev, The security of practical quantum key distribution, *Rev. Mod. Phys.* **81**, 1301 (2009).
- [3] S. Pirandola, U. L. Andersen, L. Banchi, M. Berta, D. Bunandar, R. Colbeck, D. Englund, T. Gehring, C. Lupo, C. Ottaviani, J. L. Pereira, M. Razavi, J. S. Shaari, M. Tomamichel, V. C. Usenko, G. Vallone, P. Villoresi, and P. Wallden, Advances in quantum cryptography, *Adv. Opt. Photon.* **12**, 1012 (2020).
- [4] C. H. Bennett and G. Brassard, Proceedings of the IEEE international conference on computers, systems and signal processing (IEEE Press, 1984, New York, 1984) pp. 175–179.
- [5] A. K. Ekert, Quantum cryptography based on Bell's theorem, *Phys. Rev. Lett.* **67**, 661 (1991).
- [6] C. H. Bennett, F. Bessette, G. Brassard, L. Salvail, and J. Smolin, Experimental quantum cryptography, *Journal of Cryptology* **5**, 3 (1992).
- [7] J.-Y. Wang, B. Yang, S.-K. Liao, L. Zhang, Q. Shen, X.-F. Hu, J.-C. Wu, S.-J. Yang, H. Jiang, Y.-L. Tang, B. Zhong, H. Liang, W.-Y. Liu, Y.-H. Hu, Y.-M. Huang, B. Qi, J.-G. Ren, G.-S. Pan, J. Yin, J.-J. Jia, Y.-A. Chen, K. Chen, C.-Z. Peng, and J.-W. Pan, Direct and full-scale experimental verifications towards ground-satellite quantum key distribution, *Nature Photonics* **7**, 387 (2013).
- [8] T. C. Ralph, Continuous variable quantum cryptography, *Phys. Rev. A* **61**, 010303 (1999).
- [9] M. Hillery, Quantum cryptography with squeezed states, *Phys. Rev. A* **61**, 022309 (2000).
- [10] N. J. Cerf, M. Lévy, and G. V. Assche, Quantum distribution of gaussian keys using squeezed states, *Phys. Rev. A* **63**, 052311 (2001).
- [11] F. Grosshans and P. Grangier, Continuous variable quantum cryptography using coherent states, *Phys. Rev. Lett.* **88**, 057902 (2002).
- [12] F. Grosshans, G. Van Assche, J. Wenger, R. Brouri, N. J. Cerf, and P. Grangier, Quantum key distribution

- using gaussian-modulated coherent states, *Nature* **421**, 238 (2003).
- [13] C. Weedbrook, S. Pirandola, R. García-Patrón, N. J. Cerf, T. C. Ralph, J. H. Shapiro, and S. Lloyd, Gaussian quantum information, *Rev. Mod. Phys.* **84**, 621 (2012).
- [14] A. Leverrier, R. García-Patrón, R. Renner, and N. J. Cerf, Security of continuous-variable quantum key distribution against general attacks, *Phys. Rev. Lett.* **110**, 030502 (2013).
- [15] A. Leverrier, Composable security proof for continuous-variable quantum key distribution with coherent states, *Phys. Rev. Lett.* **114**, 070501 (2015).
- [16] A. Leverrier, Security of continuous-variable quantum key distribution via a gaussian de finetti reduction, *Phys. Rev. Lett.* **118**, 200501 (2017).
- [17] R. Renner and J. I. Cirac, de finetti representation theorem for infinite-dimensional quantum systems and applications to quantum cryptography, *Phys. Rev. Lett.* **102**, 110504 (2009).
- [18] P. W. Shor and J. Preskill, Simple proof of security of the bb84 quantum key distribution protocol, *Phys. Rev. Lett.* **85**, 441 (2000).
- [19] S. L. Braunstein and S. Pirandola, Side-channel-free quantum key distribution, *Phys. Rev. Lett.* **108**, 130502 (2012).
- [20] H.-K. Lo, M. Curty, and B. Qi, Measurement-device-independent quantum key distribution, *Phys. Rev. Lett.* **108**, 130503 (2012).
- [21] S. Pirandola, C. Ottaviani, G. Spedalieri, C. Weedbrook, S. L. Braunstein, S. Lloyd, T. Gehring, C. S. Jacobsen, and U. L. Andersen, High-rate measurement-device-independent quantum cryptography, *Nature Photonics* **9**, 397 (2015).
- [22] Z. Li, Y.-C. Zhang, F. Xu, X. Peng, and H. Guo, Continuous-variable measurement-device-independent quantum key distribution, *Phys. Rev. A* **89**, 052301 (2014).
- [23] X.-C. Ma, S.-H. Sun, M.-S. Jiang, M. Gui, and L.-M. Liang, Gaussian-modulated coherent-state measurement-device-independent quantum key distribution, *Phys. Rev. A* **89**, 042335 (2014).
- [24] G. S. Agarwal and K. Tara, Nonclassical properties of states generated by the excitations on a coherent state, *Phys. Rev. A* **43**, 492 (1991).
- [25] A. Kitagawa, M. Takeoka, M. Sasaki, and A. Chefles, Entanglement evaluation of non-gaussian states generated by photon subtraction from squeezed states, *Phys. Rev. A* **73**, 042310 (2006).
- [26] A. Ourjoumtsev, A. Dantan, R. Tualle-Broui, and P. Grangier, Increasing entanglement between gaussian states by coherent photon subtraction, *Phys. Rev. Lett.* **98**, 030502 (2007).
- [27] H. Takahashi, J. S. Neergaard-Nielsen, M. Takeuchi, M. Takeoka, K. Hayasaka, A. Furusawa, and M. Sasaki, Entanglement distillation from gaussian input states, *Nature Photonics* **4**, 178 (2010).
- [28] S. L. Zhang and P. van Loock, Distillation of mixed-state continuous-variable entanglement by photon subtraction, *Phys. Rev. A* **82**, 062316 (2010).
- [29] C. Navarrete-Benlloch, R. García-Patrón, J. H. Shapiro, and N. J. Cerf, Enhancing quantum entanglement by photon addition and subtraction, *Phys. Rev. A* **86**, 012328 (2012).
- [30] T. Opatrny, G. Kurizki, and D.-G. Welsch, Improvement on teleportation of continuous variables by photon subtraction via conditional measurement, *Phys. Rev. A* **61**, 032302 (2000).
- [31] F. Dell'Anno, S. De Siena, L. Albano, and F. Illuminati, Continuous-variable quantum teleportation with non-gaussian resources, *Phys. Rev. A* **76**, 022301 (2007).
- [32] Y. Yang and F.-L. Li, Entanglement properties of non-gaussian resources generated via photon subtraction and addition and continuous-variable quantum-teleportation improvement, *Phys. Rev. A* **80**, 022315 (2009).
- [33] X.-x. Xu, Enhancing quantum entanglement and quantum teleportation for two-mode squeezed vacuum state by local quantum-optical catalysis, *Phys. Rev. A* **92**, 012318 (2015).
- [34] L. Hu, Z. Liao, and M. S. Zubairy, Continuous-variable entanglement via multiphoton catalysis, *Phys. Rev. A* **95**, 012310 (2017).
- [35] S. Wang, L.-L. Hou, X.-F. Chen, and X.-F. Xu, Continuous-variable quantum teleportation with non-gaussian entangled states generated via multiple-photon subtraction and addition, *Phys. Rev. A* **91**, 063832 (2015).
- [36] C. Kumar and S. Arora, Success probability and performance optimization in non-gaussian continuous-variable quantum teleportation, *Phys. Rev. A* **107**, 012418 (2023).
- [37] C. Kumar, M. Sharma, and S. Arora, Continuous variable quantum teleportation in a dissipative environment: Comparison of non-gaussian operations before and after noisy channel, *Advanced Quantum Technologies* **7**, 2300344 (2024).
- [38] P. Huang, G. He, J. Fang, and G. Zeng, Performance improvement of continuous-variable quantum key distribution via photon subtraction, *Phys. Rev. A* **87**, 012317 (2013).
- [39] H.-X. Ma, P. Huang, D.-Y. Bai, S.-Y. Wang, W.-S. Bao, and G.-H. Zeng, Continuous-variable measurement-device-independent quantum key distribution with photon subtraction, *Phys. Rev. A* **97**, 042329 (2018).
- [40] C. Kumar, J. Singh, S. Bose, and Arvind, Coherence-assisted non-gaussian measurement-device-independent quantum key distribution, *Phys. Rev. A* **100**, 052329 (2019).
- [41] Y. Guo, W. Ye, H. Zhong, and Q. Liao, Continuous-variable quantum key distribution with non-gaussian quantum catalysis, *Phys. Rev. A* **99**, 032327 (2019).
- [42] W. Ye, H. Zhong, Q. Liao, D. Huang, L. Hu, and Y. Guo, Improvement of self-referenced continuous-variable quantum key distribution with quantum photon catalysis, *Opt. Express* **27**, 17186 (2019).
- [43] L. Hu, M. Al-amri, Z. Liao, and M. S. Zubairy, Continuous-variable quantum key distribution with non-gaussian operations, *Phys. Rev. A* **102**, 012608 (2020).
- [44] R. Birrittella, J. Mimih, and C. C. Gerry, Multiphoton quantum interference at a beam splitter and the approach to heisenberg-limited interferometry, *Phys. Rev. A* **86**, 063828 (2012).
- [45] R. Carranza and C. C. Gerry, Photon-subtracted two-mode squeezed vacuum states and applications to quantum optical interferometry, *J. Opt. Soc. Am. B* **29**, 2581 (2012).
- [46] D. Braun, P. Jian, O. Pinel, and N. Treps, Precision measurements with photon-subtracted or photon-added gaussian states, *Phys. Rev. A* **90**, 013821 (2014).
- [47] Y. Ouyang, S. Wang, and L. Zhang, Quantum optical

- interferometry via the photon-added two-mode squeezed vacuum states, *J. Opt. Soc. Am. B* **33**, 1373 (2016).
- [48] H. Zhang, W. Ye, C. Wei, Y. Xia, S. Chang, Z. Liao, and L. Hu, Improved phase sensitivity in a quantum optical interferometer based on multiphoton catalytic two-mode squeezed vacuum states, *Phys. Rev. A* **103**, 013705 (2021).
- [49] S.-H. Tan, B. I. Erkmen, V. Giovannetti, S. Guha, S. Lloyd, L. Maccone, S. Pirandola, and J. H. Shapiro, Quantum illumination with gaussian states, *Phys. Rev. Lett.* **101**, 253601 (2008).
- [50] E. D. Lopaeva, I. Ruo Berchera, I. P. Degiovanni, S. Olivares, G. Brida, and M. Genovese, Experimental realization of quantum illumination, *Phys. Rev. Lett.* **110**, 153603 (2013).
- [51] C. Kumar, Rishabh, and S. Arora, Realistic non-gaussian-operation scheme in parity-detection-based mach-zehnder quantum interferometry, *Phys. Rev. A* **105**, 052437 (2022).
- [52] C. Kumar, Rishabh, and S. Arora, Enhanced phase estimation in parity-detection-based mach-zehnder interferometer using non-gaussian two-mode squeezed thermal input state, *Annalen der Physik* **535**, 2300117 (2023).
- [53] C. Kumar, Rishabh, M. Sharma, and S. Arora, Parity-detection-based mach-zehnder interferometry with coherent and non-gaussian squeezed vacuum states as inputs, *Phys. Rev. A* **108**, 012605 (2023).
- [54] Y. Zhao, Y. Zhang, B. Xu, S. Yu, and H. Guo, Continuous-variable measurement-device-independent quantum key distribution with virtual photon subtraction, *Phys. Rev. A* **97**, 042328 (2018).
- [55] Y.-H. Zhou, S.-F. Qin, W.-M. Shi, and Y.-G. Yang, Continuous variable measurement-device-independent quantum key distribution based on photon subtraction and optical amplifiers, *Optik* **242**, 166826 (2021).
- [56] Y. Wang, S. Zou, Y. Mao, and Y. Guo, Improving underwater continuous-variable measurement-device-independent quantum key distribution via zero-photon catalysis, *Entropy* **22**, 10.3390/e22050571 (2020).
- [57] P. Huang, G. He, J. Fang, and G. Zeng, Performance improvement of continuous-variable quantum key distribution via photon subtraction, *Phys. Rev. A* **87**, 012317 (2013).
- [58] Y. Guo, Q. Liao, Y. Wang, D. Huang, P. Huang, and G. Zeng, Performance improvement of continuous-variable quantum key distribution with an entangled source in the middle via photon subtraction, *Phys. Rev. A* **95**, 032304 (2017).
- [59] Z. Li, Y. Zhang, X. Wang, B. Xu, X. Peng, and H. Guo, Non-gaussian postselection and virtual photon subtraction in continuous-variable quantum key distribution, *Phys. Rev. A* **93**, 012310 (2016).
- [60] C. Ottaviani, G. Spedalieri, S. L. Braunstein, and S. Pirandola, Continuous-variable quantum cryptography with an untrusted relay: Detailed security analysis of the symmetric configuration, *Phys. Rev. A* **91**, 022320 (2015).
- [61] F. Grosshans, N. J. Cerf, J. Wenger, R. Tualle-Brouiri, and P. Grangier, Virtual entanglement and reconciliation protocols for quantum cryptography with continuous variables, *Quantum Info. Comput.* **3**, 535–552 (2003).
- [62] C. Weedbrook, A. M. Lance, W. P. Bowen, T. Symul, T. C. Ralph, and P. K. Lam, Quantum cryptography without switching, *Phys. Rev. Lett.* **93**, 170504 (2004).
- [63] I. Devetak and A. Winter, Distillation of secret key and entanglement from quantum states, *Proceedings of the Royal Society A: Mathematical, Physical and Engineering Sciences* **461**, 207 (2005).
- [64] F. Grasselli, Beyond point-to-point quantum key distribution, in *Quantum Cryptography: From Key Distribution to Conference Key Agreement* (Springer International Publishing, Cham, 2021) pp. 83–104.
- [65] S.-K. Liao, W.-Q. Cai, W.-Y. Liu, L. Zhang, Y. Li, J.-G. Ren, J. Yin, Q. Shen, Y. Cao, Z.-P. Li, F.-Z. Li, X.-W. Chen, L.-H. Sun, J.-J. Jia, J.-C. Wu, X.-J. Jiang, J.-F. Wang, Y.-M. Huang, Q. Wang, Y.-L. Zhou, L. Deng, T. Xi, L. Ma, T. Hu, Q. Zhang, Y.-A. Chen, N.-L. Liu, X.-B. Wang, Z.-C. Zhu, C.-Y. Lu, R. Shu, C.-Z. Peng, J.-Y. Wang, and J.-W. Pan, Satellite-to-ground quantum key distribution, *Nature* **549**, 43 (2017).
- [66] R. García-Patrón and N. J. Cerf, Unconditional optimality of gaussian attacks against continuous-variable quantum key distribution, *Phys. Rev. Lett.* **97**, 190503 (2006).
- [67] F. Laudenbach, C. Pacher, C.-H. F. Fung, A. Poppe, M. Peev, B. Schrenk, M. Hentschel, P. Walther, and H. Hübel, Continuous-variable quantum key distribution with gaussian modulation—the theory of practical implementations, *Advanced Quantum Technologies* **1**, 1800011 (2018).
- [68] H. Vahlbruch, M. Mehmet, K. Danzmann, and R. Schnabel, Detection of 15 db squeezed states of light and their application for the absolute calibration of photoelectric quantum efficiency, *Phys. Rev. Lett.* **117**, 110801 (2016).
- [69] C. Silberhorn, T. C. Ralph, N. Lütkenhaus, and G. Leuchs, Continuous variable quantum cryptography: Beating the 3 db loss limit, *Phys. Rev. Lett.* **89**, 167901 (2002).
- [70] D. Dequal, L. Trigo Vidarte, V. Roman Rodriguez, G. Vallone, P. Villoresi, A. Leverrier, and E. Diamanti, Feasibility of satellite-to-ground continuous-variable quantum key distribution, *npj Quantum Information* **7**, 3 (2021).
- [71] Y. Guo, W. Ye, H. Zhong, and Q. Liao, Continuous-variable quantum key distribution with non-gaussian quantum catalysis, *Phys. Rev. A* **99**, 032327 (2019).
- [72] H. Zhong, Y. Guo, Y. Mao, W. Ye, and D. Huang, Virtual zero-photon catalysis for improving continuous-variable quantum key distribution via gaussian post-selection, *Scientific Reports* **10**, 17526 (2020).
- [73] J. Huang, W. Ye, C. Liu, Q. Kuang, and F. Jia, Underwater quantum key distribution with continuous-variable via photon additions, *Results in Physics* **54**, 107136 (2023).
- [74] M. Hillery, Sum and difference squeezing of the electromagnetic field, *Phys. Rev. A* **40**, 3147 (1989).
- [75] L. Mandel, Sub-poissonian photon statistics in resonance fluorescence, *Opt. Lett.* **4**, 205 (1979).
- [76] C. T. Lee, Many-photon antibunching in generalized pair coherent states, *Phys. Rev. A* **41**, 1569 (1990).
- [77] Arvind and N. Mukunda, Bell's inequalities, multiphoton states and phase space distributions, *Physics Letters A* **259**, 421 (1999).
- [78] C. Kumar, G. Saxena, and Arvind, Continuous-variable clausen-horne bell-type inequality: A tool to unearth the nonlocality of continuous-variable quantum-optical systems, *Phys. Rev. A* **103**, 042224 (2021).
- [79] M. G. Genoni, M. G. A. Paris, and K. Banaszek, Quantifying the non-gaussian character of a quantum state

- by quantum relative entropy, *Phys. Rev. A* **78**, 060303 (2008).
- [80] Arvind, B. Dutta, N. Mukunda, and R. Simon, The real symplectic groups in quantum mechanics and optics, *Pramana* **45**, 471 (1995).
- [81] S. L. Braunstein and P. van Loock, Quantum information with continuous variables, *Rev. Mod. Phys.* **77**, 513 (2005).
- [82] G. Adesso and F. Illuminati, Entanglement in continuous-variable systems: recent advances and current perspectives, *J. Phys. A* **40**, 7821 (2007).
- [83] G. Adesso, S. Ragy, and A. R. Lee, Continuous variable quantum information: Gaussian states and beyond, *Open Syst. Inf. Dyn.* **21**, 1440001, 47 (2014).
- [84] Arvind, B. Dutta, C. L. Mehta, and N. Mukunda, Squeezed states, metaplectic group, and operator möbius transformations, *Phys. Rev. A* **50**, 39 (1994).
- [85] Arvind, B. Dutta, N. Mukunda, and R. Simon, Two-mode quantum systems: Invariant classification of squeezing transformations and squeezed states, *Phys. Rev. A* **52**, 1609 (1995).
- [86] S. Olivares, Quantum optics in the phase space, *The European Physical Journal Special Topics* **203**, 3 (2012).